

NMR, magnetization, and heat capacity studies of the uniform spin- $\frac{1}{2}$ chain compound $\text{Bi}_6\text{V}_3\text{O}_{16}$

T. Chakrabarty,^{1,2,*} I. Heinmaa,^{1,†} V. Yu. Verchenko,^{1,3,‡} P. L. Paulose,^{2,§} and R. Stern^{1,¶}

¹National Institute of Chemical Physics and Biophysics, 12618 Tallinn, Estonia

²Tata Institute of Fundamental Research, Homi Bhabha Road, Colaba, 400005 Mumbai, India

³Department of Chemistry, Lomonosov Moscow State University, 119991 Moscow, Russia

(Received 29 January 2019; Revised 1 August 2019)

We report the local (NMR) and bulk (magnetization and heat capacity) properties of the vanadium based spin- $\frac{1}{2}$ uniform spin chain compound $\text{Bi}_6\text{V}_3\text{O}_{16}$ ($\text{Bi}_4\text{V}_2\text{O}_{10.66}$). In the low-temperature α phase, the magnetic ions (V^{4+}) are arranged in one-dimensional chains. The magnetic susceptibility shows a broad maximum around 50 K signifying a short-range magnetic order. Heat capacity measurements also reveal low-dimensional magnetism. The ^{51}V magic angle spinning nuclear magnetic resonance measurements clearly show that the magnetic V^{4+} and non-magnetic V^{5+} species are located on different crystallographic sites with no mixed occupation. The spin susceptibility calculated from the shift of the ^{51}V NMR spectra reproduces the behavior observed in magnetic susceptibility and agrees well with the spin- $\frac{1}{2}$ uniform spin chain model with $J = 113(5)$ K.

PACS numbers: 76.60.-k, 75.47.Lx, 75.50.Ee

I. INTRODUCTION

Magnetism in one-dimensional (1D) Heisenberg antiferromagnetic (AFM) spin systems has remained an area of wide interest in condensed-matter physics since 1970s.^{1,2} This is mainly due to the rich physics such spin chains exhibit. Furthermore, these systems are tractable from both theoretical^{3,4} and computational⁵⁻⁷ starting points. The prime interest here is the innate strong quantum fluctuations which lead to the suppression of magnetic long range ordering.⁸ The nature of the ground state in these systems depends on the value of spin S and relative strength and sign (AFM or ferromagnetic) of their coupling J . The generic magnetic Hamiltonian describing an $S = \frac{1}{2}$ Heisenberg chain can be written as $H = J \sum_i S_i S_{i+1}$, where J is the intrachain coupling constant between the nearest-neighbor spins. A uniform half-integer spin chain with AFM interactions exhibits a gapless ground state.⁹⁻¹⁹ In the case of an AFM alternating Heisenberg chain, the AFM exchange constants (J_1 and J_2) between the two nearest-neighbor spins are unequal ($J_1 \neq J_2$; $J_1, J_2 > 0$), and they alternate from bond to bond along the chain with an alteration parameter $\alpha = J_2/J_1$. In the case of an alternating chain, interactions for half-integer spins result in the opening of a gap via either frustration due to the next-nearest-neighbor AFM exchange or dimerization due to the alternating coupling to nearest neighbors along the chain.²⁰⁻²⁹ Many $S = \frac{1}{2}$ chain systems have already been reported, and their characteristics have been interpreted on the basis of such a model. Some of the most renowned examples in this category are $\text{CuCl}_2 \cdot 2\text{N}(\text{C}_5\text{D}_5)$,⁹ KCuF_3 ,¹⁰⁻¹² Sr_2CuO_3 ,¹³ $\text{CuSO}_4 \cdot 5\text{H}_2\text{O}$,¹⁴ $\text{Ba}_2\text{Cu}(\text{PO}_4)_2$,¹⁵ and, recently, $(\text{NO})[\text{Cu}(\text{NO}_3)_3]$ ¹⁶⁻¹⁸ and $\text{Cs}_4\text{CuSb}_2\text{Cl}_{12}$ ¹⁹ for uniform and $\text{Cu}(\text{NO}_3)_2 \cdot 2.5\text{H}_2\text{O}$,^{21,22} $(\text{VO})_2\text{P}_2\text{O}_7$,²³⁻²⁶ $\text{CaCuGe}_2\text{O}_6$,²⁷ AgVOAsO_4 ²⁸, and $\text{Cu}_3(\text{MoO}_4)(\text{OH})_4$ ²⁹ for alternating $S = \frac{1}{2}$ Heisenberg spin chains.

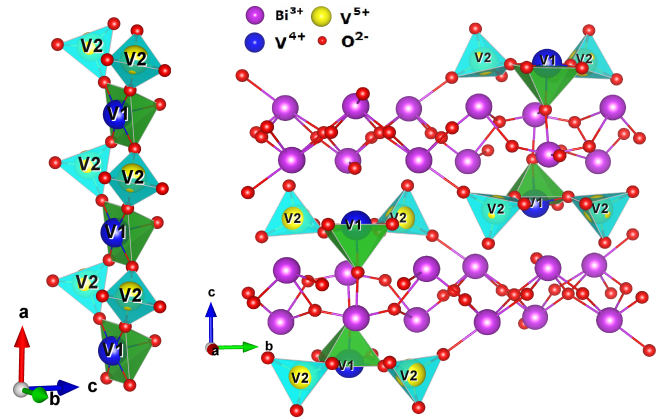


Figure 1: Left: Possible interaction path between the magnetic V^{4+} ions in $\text{Bi}_6\text{V}_3\text{O}_{16}$ mediated via nonmagnetic V^{5+} ions and oxygen. Right: Top view of the chains separated by Bi-O layers.

Our motivation is to explore new low-dimensional magnetic oxides with the intention of unraveling novel magnetic properties. In this paper we report the bulk and local (NMR) studies of the vanadium-based $S = \frac{1}{2}$ uniform spin chain compound $\text{Bi}_6\text{V}_3\text{O}_{16}$ (often described also as $\text{Bi}_4\text{V}_2\text{O}_{10.66}$) at low temperatures. This system is a member of the well-known pseudo binary oxide systems $\text{Bi}_2\text{O}_3\text{-V}_2\text{O}_5$, which received significant interest because of their different structural varieties and rich functional properties,^{30,31} which led also to a very efficient bismuth-metal-vanadia (BiMeVOX) family of anionic conductors.^{32,33} These systems belong to or are derived from the Aurivillius family.^{34,35} They exhibit three polymorphs, α , β , and γ , each associated with a different temperature range, where the α phase is the low-temperature one. One of these Aurivillius vanadates, $\text{Bi}_4\text{V}_2\text{O}_{10}$ which contains all the vanadium ions in the

V^{4+} oxidation state, was studied thoroughly via crystal structure, electron diffraction, and thermodynamic properties about two decades ago.^{36,37} In the α phase of $\text{Bi}_4\text{V}_2\text{O}_{10}$, the magnetic V^{4+} ions are arranged in a 1D chain along the a direction of the unit cell (see Fig. 1; VESTA software³⁸ was used for crystal structure visualization). It was also proposed by Satto *et al.*³⁷ that $\alpha\text{-Bi}_4\text{V}_2\text{O}_{10}$ transforms to $\alpha\text{-Bi}_6\text{V}_3\text{O}_{16}$ after oxidation upon exposure to air at room temperature. The orientation of the magnetic V^{4+} ions in 1D chains remains intact in the crystal structure of the α phase of $\text{Bi}_6\text{V}_3\text{O}_{16}$, which is best described by $\text{V}_3\text{O}_{16}^{6-}$ ribbons running along the a axis and containing units built up from a pyramid (V^{4+}) and two tetrahedra (V^{5+}).^{39,40} This is one of the few systems found so far in nature where the extended superexchange interaction takes place by the overlap of d_{xy} (via the oxygen p) orbitals of d_1 electrons (t_{2g}) of V^{4+} ions rather than the $d_{x^2-y^2}$ orbitals of e_g electrons in Cu-based systems, with an exchange coupling (J/k_B) as high as ~ 100 K. Very recently, magnetic properties and charge ordering were reported for another related compound, $\text{Bi}_{3.6}\text{V}_2\text{O}_{10}$,^{41,42} which also belongs to the aforementioned Aurivillius family. However, a detailed investigation of the bulk and local properties with a proper theoretical model has not been carried out for any of these magnetic Aurivillius vanadates. This leads to the the primary sources of motivation for our present work.

II. SAMPLE PREPARATION, CRYSTAL STRUCTURE, AND EXPERIMENTAL DETAILS

$\text{Bi}_6\text{V}_3\text{O}_{16}$ is an orthorhombic system and crystallizes in the $Pnma$ space group.³⁹ The low-temperature phase of $\text{Bi}_6\text{V}_3\text{O}_{16}$ was synthesized by mixing stoichiometric amounts of Bi_2O_3 (Alfa Aesar, 99.99%) and VO_2 . VO_2 was prepared through the reaction of an equimolar mixture of V_2O_5 and V_2O_3 at 680°C for 18 h under vacuum. V_2O_3 was obtained by reducing V_2O_5 (99.99%, Aldrich) under hydrogen flow at 800°C . The mixture of Bi_2O_3 and VO_2 was then pelletized and placed in a quartz ampule sealed in vacuum ($< 10^{-5}$ mbar). The ampule was annealed at 550°C for 48 h. This process was repeated three times with intermediate grinding and mixing. The last round of heating was performed at 620°C for 36 h. After a few weeks of exposure in open air, $\text{Bi}_4\text{V}_2\text{O}_{10}$ self-oxidized into $\text{Bi}_6\text{V}_3\text{O}_{16}$, and its color changed from black to dark brown. A similar transformation was observed previously by Satto *et al.*³⁷

Energy dispersive x-ray (EDX) microanalysis show an elemental ratio of bismuth and vanadium of $\text{Bi}:\text{V} \simeq 2 : 1$ (see Fig. 2).

X-ray diffraction (XRD) patterns were collected using a PANalytical X'Pert³ Powder x-ray diffractometer (Cu $K\alpha$ radiation, $\lambda = 1.54182 \text{ \AA}$). The Rietveld refinement against the XRD data was carried out using the JANA2006 software⁴³ (see Fig. 3). The XRD pattern shows a single phase of $\text{Bi}_6\text{V}_3\text{O}_{16}$ (space group:

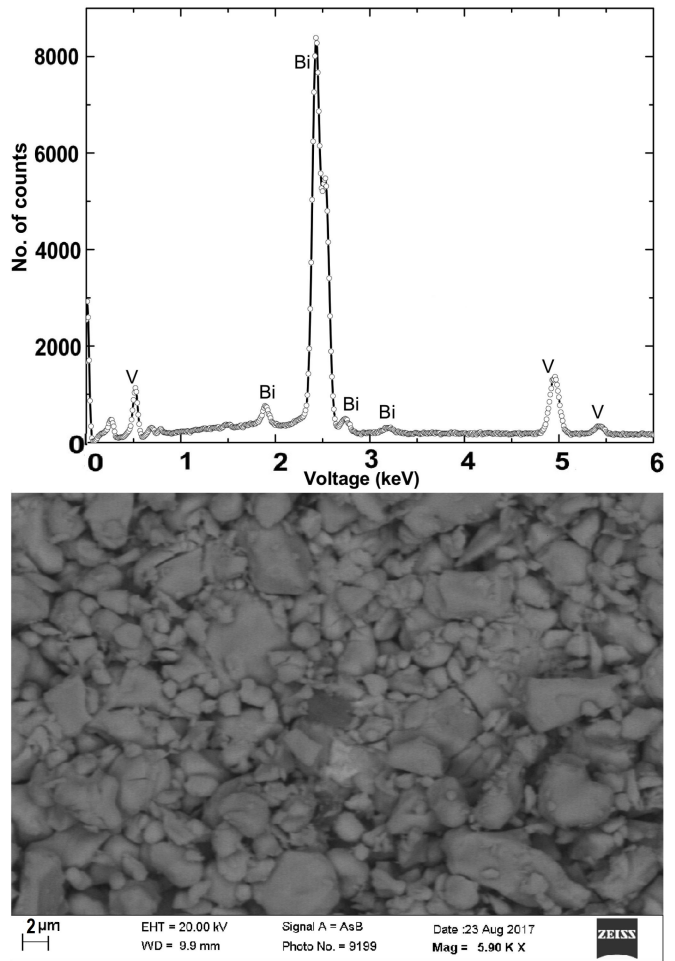


Figure 2: EDX spectrum (top) and SEM image (bottom) of polycrystalline $\text{Bi}_6\text{V}_3\text{O}_{16}$.

$Pnma$ (62), $a = 5.47124(3) \text{ \AA}$, $b = 17.25633(8) \text{ \AA}$, $c = 14.92409(6) \text{ \AA}$). The ratio of $c/(b/3) \simeq 2.6$ obtained from the refinement is consistent with the previous study carried out on single crystals of the α phase of $\text{Bi}_6\text{V}_3\text{O}_{16}$.⁴⁰ The refined atomic coordinates of $\text{Bi}_6\text{V}_3\text{O}_{16}$ are given in Table I.

The thermogravimetric analysis (TGA) was carried out to heat $\text{Bi}_6\text{V}_3\text{O}_{16}$ and to oxidize it while observing the weight change (see Fig. 4). After the full oxidation, $\text{Bi}_6\text{V}_3\text{O}_{16}$ ($\text{Bi}_4\text{V}_2\text{O}_{10.66}$) should transform into $\text{Bi}_4\text{V}_2\text{O}_{11}$ in which all vanadium ions are in the V^{5+} oxidation state. In our experiments, we observed three major temperature effects. The first one at 550 K is due to the oxygen intake, the second one at 720 K is due to the $\alpha \rightarrow \beta$ transition, and the last one at 860 K is due to the $\beta \rightarrow \gamma$ phase transition. The calculated mass change during the phase transition at 550 K is 0.65%, which is close to what is expected from the oxidation of $\text{Bi}_6\text{V}_3\text{O}_{16}$ to $\text{Bi}_4\text{V}_2\text{O}_{11}$ (0.5%).

Analysis of the V-V interaction path (see Fig. 1) reveals that two vanadium ions from crystallographic site V1 (magnetic V^{4+}) are connected by two oxygen ions

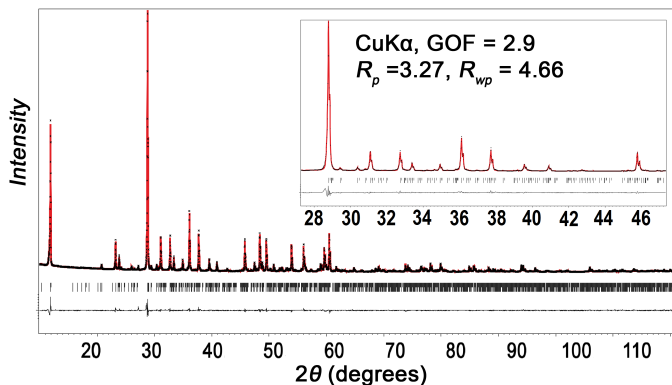


Figure 3: Experimental (black points) and calculated (red line) powder XRD patterns of $\text{Bi}_6\text{V}_3\text{O}_{16}$. Positions of peaks are given by black ticks, and the difference plot is shown by the black line in the bottom part.

| Atoms | Coordinates | | | TDP |
|---------|-------------|-------------|-------------|------------------------|
| | x/a | y/b | z/c | $B_{iso} (\text{Å}^2)$ |
| Bi1(4c) | 0.2004(7) | 0.250 | 0.31668(17) | 2.13(7) |
| Bi2(4c) | 0.2519(7) | 0.250 | 0.66949(17) | 2.08(8) |
| Bi3(8d) | 0.2368(4) | 0.41275(14) | 0.83414(13) | 1.98(6) |
| Bi4(8d) | 0.2835(5) | 0.42850(12) | 0.16763(14) | 2.25(6) |
| V1(4c) | 0.246(3) | 0.250 | 0.0331(7) | 4.1(3) |
| V2(8d) | 0.265(2) | 0.3864(4) | 0.4874(6) | 3.8(2) |
| O1(4c) | -0.030(4) | -0.0171(15) | 0.2391(15) | 0.5(2) |
| O2(8d) | 0.127(4) | 0.3523(13) | 0.2921(11) | 0.5(2) |
| O3(8d) | 0.010(6) | 0.323(2) | 0.7464(15) | 0.5(2) |
| O4(8d) | -0.018(6) | 0.3226(17) | 0.0536(10) | 0.5(2) |
| O5(4a) | -0.015(6) | 0.331(2) | 0.4704(9) | 0.5(2) |
| O6(8d) | 0.287(4) | 0.4056(14) | 0.5912(10) | 0.5(2) |
| O7(8d) | 0.207(5) | 0.4749(11) | 0.4325(10) | 0.5(2) |
| O8(8d) | 0.316(6) | 0.250 | 0.1752(16) | 0.5(2) |
| O9(8d) | 0.178(6) | 0.250 | 0.8582(15) | 0.5(2) |

Table I: Atomic coordinates and thermal displacement parameters in the crystal structure of $\text{Bi}_6\text{V}_3\text{O}_{16}$.

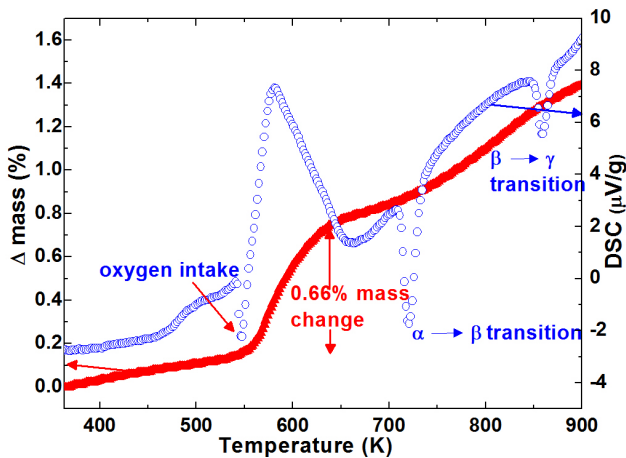


Figure 4: Temperature dependence of the mass change and the heat flow during heating of $\text{Bi}_6\text{V}_3\text{O}_{16}$ in the TGA experiment.

| Bonds | Description | Value (Å) |
|-------|-------------|-----------|
| V1-O5 | intrachain | 1.92 |
| O5-V2 | intrachain | 1.82 |
| V2-O4 | intrachain | 1.73 |
| O4-V1 | intrachain | 1.94 |

Table II: Bond lengths between various vanadium-oxygen linkages along the a direction of the 1D chain in $\text{Bi}_6\text{V}_3\text{O}_{16}$

| Angles | Description | Value (deg) |
|----------|-------------|-------------|
| V1-O5-V2 | intrachain | 163.97 |
| O5-V2-O4 | intrachain | 101.07 |
| V2-O4-V1 | intrachain | 150.15 |

Table III: Bond angles between various vanadium-oxygen linkages in $\text{Bi}_6\text{V}_3\text{O}_{16}$

and one vanadium from crystallographic site V2 (non-magnetic V^{5+}). The type of magnetic interaction between the V^{4+} ions is hence extended to superexchange ($\text{V}^{4+}-\text{O}^{2-}-\text{V}^{5+}-\text{O}^{2-}-\text{V}^{4+}$). The V-V distances are equal along the chains. V^{4+} and V^{5+} ions are in the pyramidal and tetrahedral environments of oxygens, respectively (see Fig. 1). The bond distances and bond angles along the V-V interaction path for $\text{Bi}_6\text{V}_3\text{O}_{16}$ are listed in Tables II and III, respectively. From the structural point of view the system resembles a $S = \frac{1}{2}$ uniform 1D Heisenberg chain.

Recent reports⁴² on the crystallographic data for the similar compounds $\text{Bi}_4\text{V}_2\text{O}_{10.2}$ and $\text{Bi}_{3.6}\text{V}_2\text{O}_{10}$ document that V^{4+} ions occupy the V1 site, and V^{5+} ions are placed on the V2 sites. $\text{Bi}_6\text{V}_3\text{O}_{16}$ is derived from the same Aurivillius family, having a similar composition and preparation route. Here as well, V^{4+} ions and V^{5+} ions occupy the V1 and V2 sites, respectively.

The field (up to 14 T) and temperature (2 – 300 K) dependence of the heat capacity and magnetization M were measured using the heat capacity and vibrating-sample magnetometer options of a Quantum Design physical property measurement system, respectively.

The magic angle spinning nuclear magnetic resonance (MAS-NMR) measurements (spectra and nuclear spin-lattice relaxation times T_1) were carried out on vanadium nuclei (^{51}V gyromagnetic ratio $\gamma/2\pi = 11.1921 \text{ MHz T}^{-1}$ and nuclear spin $I = 7/2$) in a fixed field of the 4.7-T magnet using an AVANCE-II Bruker spectrometer. The spinning speed of the 1.8-mm o.d. rotor was varied between 20 and 30 kHz.⁴⁴ Typical pulse widths were varied from 4 to 2 μs . In echo sequence $\pi/2-\tau-\pi$, a rotation period between the excitation and refocusing pulses was needed, τ . By measuring NMR using this technique, the nuclear dipole-dipole interactions and chemical shift anisotropy are averaged out, and the quadrupolar interaction is partially averaged out. Thus, MAS-NMR gives finer details about the spectra. For T_1 , the speed of the rotor was 30 kHz, and the measurements were undertaken at the frequency of the isotropic shift at a given temperature. T_1 was measured by the saturation recovery method

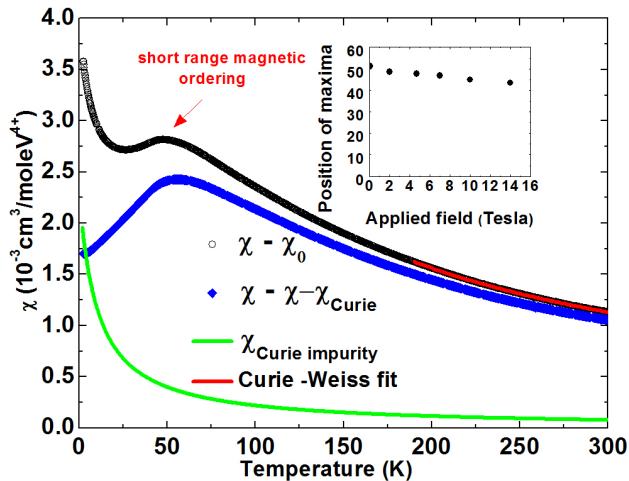


Figure 5: The temperature dependence of the susceptibility $\chi = M/H$ at $H = 4.7$ T for $\text{Bi}_6\text{V}_3\text{O}_{16}$. Black open circles are $\chi - \chi_0$ data, the green line is the low- T Curie-Weiss contribution and the blue solid diamonds show $\chi - \chi_0 - \chi_{\text{Curie}}$. The region of short-range magnetic ordering is indicated by the red arrow. The red line shows the high- T Curie-Weiss fit in the temperature range of 190 – 300 K. The inset shows the variation of the position of maximum in the magnetic susceptibility curves with the change in applied field.

using a saturation comb of fifty $\pi/2$ pulses followed by variable delay and an echo sequence for recording the intensity. For the lowest temperatures, T_1 measurements were performed in static conditions to explore the low-temperature behavior down to 4 K. The frequency shifts are given relative to the VOCl_3 reference.

III. RESULTS AND DISCUSSION

A. Magnetic susceptibility

Magnetic susceptibility $\chi = M/H$ measurements were carried out in 0.05 - 14-T applied magnetic fields. With decreasing temperature, χ follows the Curie-Weiss law and shows a broad maximum around 50 K, which indicates the presence of short-range magnetic ordering in the system. A Curie-like upturn is observed at lower temperatures, possibly arising from paramagnetic impurities. From the Curie-Weiss fit, $\chi(T) = \chi_0 + C/(T - \theta_{CW})$ in the T range 190 – 300 K (see Fig. 5), the T -independent $\chi_0 = 8.6 \times 10^{-6} \text{ cm}^3/(\text{mole V}^{4+})$, the Curie constant $C = 0.4 \text{ cm}^3\text{K}/(\text{mole V}^{4+})$, and the Curie-Weiss temperature $\theta_{CW} = -60$ K can be extracted. The negative value of θ_{CW} indicates that the dominant exchange couplings between V^{4+} ions are AFM. We also measured the electron spin resonance spectrum of the powder (X band, room temperature; not shown) and found typical g -values for a V^{4+} ion [$(g_x, g_y, g_z) = (1.93, 1.91, 1.8)$] with tiny anisotropy.

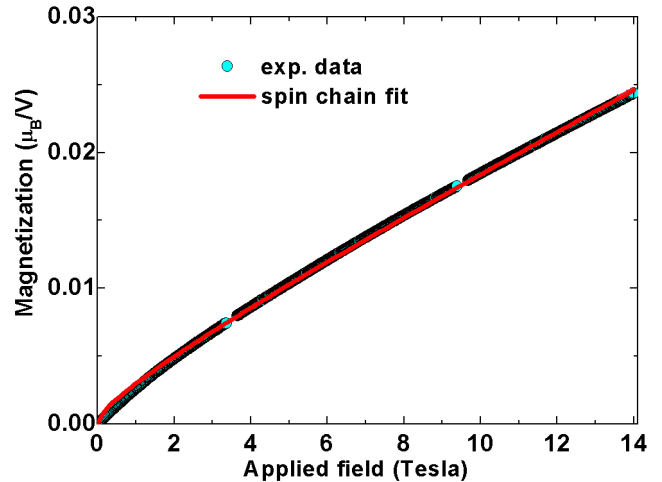


Figure 6: The experimental magnetization data of $\text{Bi}_6\text{V}_3\text{O}_{16}$ vs applied magnetic field at 1.8 K.

From our χ measurements in $\text{Bi}_6\text{V}_3\text{O}_{16}$, the value of the Curie constant ($C = 0.135 \text{ cm}^3\text{K}/\text{mole}$) is 36% of the expected value ($C = 0.375 \text{ cm}^3\text{K}/\text{mole}$) for a full $S = 1/2$ moment which indicates that only about 1/3 of the vanadium ions are magnetic, i.e., in the V^{4+} oxidation state. Earlier reports^{41,42} on similar systems ($\text{Bi}_4\text{V}_2\text{O}_{10.2}$ and $\text{Bi}_{3.6}\text{V}_2\text{O}_{10}$) suggested that V^{4+} and V^{5+} ions prefer the V1 and V2 sites respectively, namely 90% of the V1 site is occupied by V^{4+} and the rest is filled by the nonmagnetic V^{5+} , meaning that V1 site is shared by the mixed valences. From the bulk measurements, we have not acquired any evidence of the existence of site sharing in $\text{Bi}_6\text{V}_3\text{O}_{16}$.

From the $\chi(T)$ results, the Van Vleck susceptibility $\chi_{VV} = \chi_0 - \chi_{\text{core}} = 12.4 \times 10^{-5} \text{ cm}^3/\text{mole}$, where χ_{core} is the core diamagnetic susceptibility, was calculated with a value of $-11.52 \times 10^{-5} \text{ cm}^3/\text{mole f. u.}$ (here we consider the formula unit to be $\text{Bi}_2\text{VO}_{5.33}$). The low-temperature upturn in $\chi(T)$ below 20 K is attributed to the orphan spins and other extrinsic magnetic impurities.²⁹

To extract the exact magnetic susceptibility, the temperature-independent susceptibility (Van Vleck plus the core diamagnetic susceptibility) and the Curie contribution originating from the extrinsic paramagnetic impurities and/or orphan spins were subtracted from the experimentally obtained magnetic susceptibility data (see Fig. 5). The low-temperature Curie-Weiss fit gives $C = 0.022 \text{ cm}^3\text{K}/\text{mole}$, $\theta_{CW} = 10.3$ K. From the value of C we find that this contribution is about 6% of an ideal $S = 1/2$ system. After subtracting this, we find that the magnetic susceptibility saturates to a fixed value as T tends towards zero, which is expected for a gapless $S = 1/2$ uniform chain. However, to model the susceptibility with the uniform $S = 1/2$ Heisenberg chain, we rely on the MAS-NMR data below, where the spin susceptibility is manifested in a more pristine manner.

We have not observed any signature of hysteresis in the

M vs H measurements. The broad maximum observed in our system greatly resembles what was observed in similar Bi-V-O complexes reported previously.^{41,42} With the increase in the applied field, we observe that the broad maximum shifts towards lower temperatures (see the inset of Fig. 5).

In the applied field H dependence of magnetization M (see Fig. 6), we have not found any anomaly or steps indicating the presence of any gap, and the data agree well with the phenomenological expression $M^{\text{chain}}(H) = \alpha H + \beta\sqrt{H}$, with $\alpha = 1.3 \times 10^{-7}$, and $\beta = 1.65 \times 10^{-5}$.

B. Heat capacity

In the temperature dependence of heat capacity C_p , we did not detect any long range magnetic ordering (Fig. 7). In the plot of C_p/T vs. T , the broad maximum at around 55 K is observed, which does not shift under the application of external magnetic field up to 9 T. The magnetic specific heat C_m was extracted by subtracting the lattice contribution using a combination of Debye and Einstein heat capacities, C_{Debye} and C_{Einstein} , respectively:

$$C_{\text{Debye}} = C_d \times 9nR(T/\theta_d)^3 \int_0^{\theta_d/T} [x^4 e^x / (e^x - 1)^2] dx,$$

$$C_{\text{Einstein}} = 3nR \left[\sum C_{e_m} \frac{x_{E_m}^2 e^{x_{E_m}}}{(e^{x_{E_m}} - 1)^2} \right], \quad x = \frac{h\omega_E}{k_B T}.$$

In the above formula, n is the number of atoms in the primitive cell, k_B is the Boltzmann constant, θ_d is the relevant Debye temperature, and m is an index for an optical mode of vibration. In the Debye-Einstein model the total number of modes of vibration (acoustic plus optical) is equal to the total number of atoms in the formula unit. In this model we considered the ratio of the relative weights of acoustic modes and the sum of the different optical modes to be 1 : $n - 1$.

We used a single Debye and multiple (three) Einstein functions with the coefficient C_d for the relative weight of the acoustic modes of vibration and coefficients C_{e_1} , C_{e_2} , and C_{e_3} for the relative weights of the optical modes of vibration. The experimental data of the system were fitted by excluding the low-temperature region of 2 – 115 K assuming that most of the magnetic part of the heat capacity is confined within this temperature range. The fit of our experimental data to such a combination of Debye and Einstein heat capacities yields a Debye temperature of 96 K and Einstein temperatures of 130, 295, and 584 K with relative weights of $C_d : C_{e_1} : C_{e_2} : C_{e_3} = 13 : 14 : 48 : 25$.

The electronic contribution to the total heat capacity was neglected since the compound possesses an insulating ground state. Upon subtracting the lattice heat capacity with the above parameters, we obtain the magnetic contribution to the heat capacity $C_m(T)$, which, accordingly, shows a broad maximum around 50 K. The entropy change ΔS was calculated by integrating the C_m/T data (see bottom inset in Fig. 7). The entropy change is about 5.36 J K^{-1} (calculated for 1 mole), which is close to the expected value of a $S = \frac{1}{2}$ system ($R \ln 2$

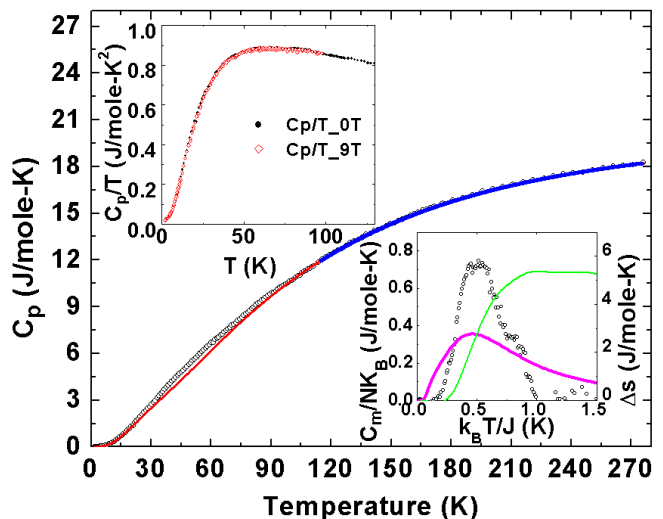


Figure 7: The temperature dependence of specific heat of $\text{Bi}_6\text{V}_3\text{O}_{16}$ in zero magnetic field; the blue points are the fit described in the text, and the red line is its extrapolation. The top inset displays the C_p/T vs T plot at 0 T (black solid circles) and 9 T (red open diamonds) magnetic fields, respectively. The bottom inset shows the magnetic contribution to the heat capacity (black open circles). The magenta line is the magnetic heat capacity contribution for the 1D uniform Heisenberg chain; the green data points (right axis) show the change in entropy ΔS with T .

$= 5.73 \text{ J/mole K}$). Although the observance of the broad maximum in the C_m vs T data indicates the 1D magnetic interaction in the system, in the temperature regime below 30 K, the magnetic heat capacity is less than 1 % of the lattice contribution, which makes the analysis of the magnetic contribution in this regime highly dependent on the model.

We have also compared C_m with the 1D Heisenberg chain model⁷ (see the magenta line in bottom inset in Fig. 7). The mismatch between our calculated C_m and the fit is not surprising as we know that an accurate estimation of C_m is nearly impossible at this temperature range as the phonon contribution (lattice part) consists of nearly 99% of the heat capacity around the peak of C_m at such a relatively high temperature.

The main findings from our heat capacity results are that we did not observe any magnetic long-range ordering in our system and C_m shows the same trend observed in χ vs T data. Both these results support the low-dimensional magnetic behavior in $\text{Bi}_6\text{V}_3\text{O}_{16}$.

C. NMR

1. Room-temperature magic angle spinning NMR

NMR is a powerful local probe to extract the static and dynamic properties of a spin system and has been extensively used on vanadia systems.⁴⁵ Fortunately, the room-

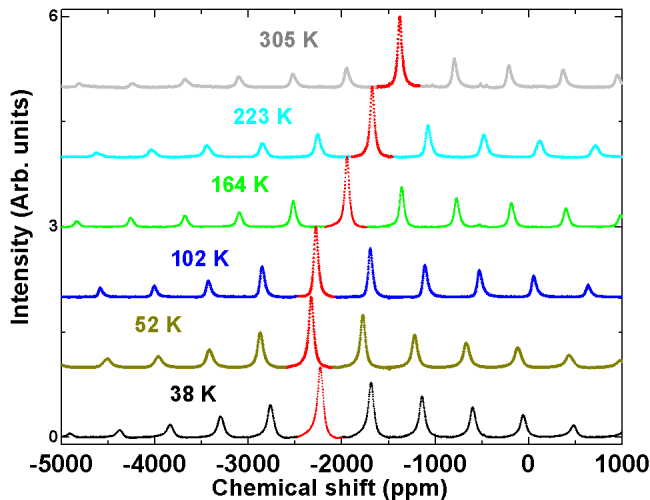


Figure 8: ^{51}V MAS-NMR spectra of $\text{Bi}_6\text{V}_3\text{O}_{16}$ measured at different temperatures in 4.7-T fixed magnetic field. The main line at the isotropic value of the magnetic shift is highlighted in red, and the rest of the peaks are spinning sidebands at multiples of the spinning frequency (30 kHz) apart from the main line.

temperature ^{51}V MAS-NMR spectrum for $\text{Bi}_6\text{V}_3\text{O}_{16}$ is known, consisting of a single line shifted to -1447 ppm at room temperature (with sample spinning speeds up to 17 kHz).⁴⁶ In our MAS spectra, we observed also only one ^{51}V line at -1382 ppm (spinning at 30 kHz; see the uppermost spectrum in Fig. 8 and the top spectrum of Fig. 9) confirming that the ^{51}V NMR signal originates entirely and from only one of the two available vanadium sites in this system.⁴⁷ As the spectral resolution is much better in the ^{51}V MAS-NMR compared to any bulk measurement or even to the static NMR data, having a single strongly shifted sharp NMR line validates the structure of $\text{Bi}_6\text{V}_3\text{O}_{16}$ here very strongly.

We have also performed room-temperature MAS-NMR measurements on $\text{Bi}_4\text{V}_2\text{O}_{11}$, the nonmagnetic parent compound of the BiMeVOX family, and compared the ^{51}V NMR signals of these two compounds under the same experimental conditions (Fig. 9). For $\text{Bi}_4\text{V}_2\text{O}_{11}$, the ^{51}V MAS-NMR line positions are also documented^{48,49}, and our results agree well with the literature. MAS-NMR results published by Delmaire *et al.*⁴⁶ showed the detection of four (three major) structurally different V^{5+} environments. The MAS-NMR results of Kim and Grey showed the detection of three different vanadiums.⁴⁹ Based on the crystal structure analysis of Mairesse *et al.*⁵⁰ and NMR studies of Kim and Grey⁴⁹ we can assign the peak at -423 ppm to the tetrahedral V^{5+} (the V1 site according to the description of Ref. 50), the peak at -509 ppm to V^{5+} in the trigonal bipyramidal environment (V2), and peaks at -491 and -497 ppm to the two different five-fold V^{5+} environments. These last two are V3a and V3b according to the report by Mairesse *et al.*;⁵⁰ however, we cannot differentiate which one is V3a and which is

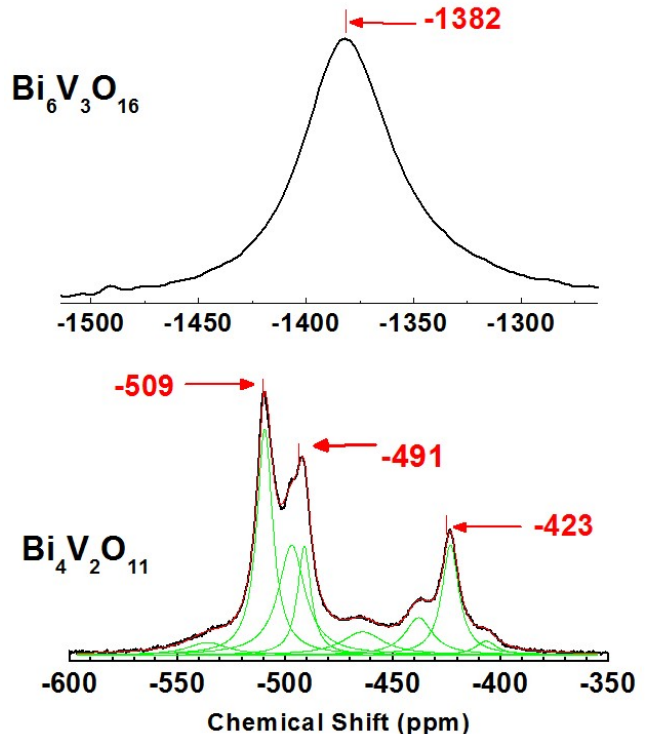


Figure 9: The top spectrum is the zoomed part of the central peak of the room-temperature (305 K) ^{51}V NMR spectrum of $\text{Bi}_6\text{V}_3\text{O}_{16}$. The bottom spectrum is the ^{51}V MAS-NMR spectrum of $\text{Bi}_4\text{V}_2\text{O}_{11}$. The black line is the experimental spectrum, which can be well fitted by several Lorentzian lines, as given by green lines; the red line is the sum of the components. The spectra were recorded on an AVANCE-III-800 spectrometer at ^{51}V resonance frequency of 210.5 MHz, using a home-built MAS probe for 1.3-mm rotors, at 50.1-kHz sample spinning speed.

V3b in our spectrum. The remaining lines with lower intensities are possibly due to the V^{5+} ions close to the ends of chains and from the $6a_m$ superstructure which was detected at low level in the XRD data of Ref. 50.

The chemical shift, the width, and relative intensity of these components are given in Table IV.

The determined aspects further validate that in the case of $\text{Bi}_6\text{V}_3\text{O}_{16}$, the possibility of V^{4+} ions occupying two different sites is clearly ruled out, as this would lead to the creation of different environments of V^{5+} ions and, consequently, different NMR lines which should get detected in MAS-NMR experiments. However, due to a strong, large hyperfine field on V^{4+} ions, the NMR signal originating from the magnetic vanadium ions could not be detected at elevated temperatures. A similar scenario was observed in many other systems such as Cs_2CuCl_4 ,⁵¹ $\text{BaCuSi}_2\text{O}_6$,⁵²⁻⁵⁴ $\text{SrCu}_2(\text{BO}_3)_2$,^{55,56} BaV_3O_8 ,⁵⁷ and $\text{Li}_2\text{ZnV}_3\text{O}_8$.⁵⁸ The example of BaV_3O_8 is most relevant in this context because BaV_3O_8 is also a 1D chain system where the signal from the magnetic V^{4+} ions was not detected, while the signal from the nonmag-

| | Frequency shift (ppm) | FWHM (ppm) | Relative intensity (%) |
|--------|-----------------------|------------|------------------------|
| Peak 1 | -423 | 10 | 15 |
| Peak 2 | -509 | 9 | 29 |
| Peak 3 | -491 | 8 | 11 |
| Peak 4 | -438 | 16 | 8 |
| Peak 5 | -407 | 12 | 2 |
| Peak 6 | -464 | 23 | 8 |
| Peak 7 | -536 | 23 | 4 |
| Peak 8 | -497 | 15 | 23 |

Table IV: The chemical shift, the width, and relative intensity of different vanadium lines in $\text{Bi}_4\text{V}_2\text{O}_{11}$ spectra.

netic V^{5+} was observed.⁵⁷

2. Low-temperature, cryoMAS NMR

The temperature dependence of ^{51}V spectra of $\text{Bi}_6\text{V}_3\text{O}_{16}$ measured using cryogenic MAS (cryoMAS) technique⁴⁴ is shown in Fig. 8. Here, we are limited to remain above $T = 20$ K to maintain the fast sample spinning, but the obtained values of the isotropic Knight shift K up to room temperature are very accurately determined, and they follow the same trend observed in $\chi(T)$. In the temperature dependence of K , a broad maximum at around 50 K is observed, similar to the $\chi(T)$ data, indicating low-dimensional, short-range magnetic ordering.

As $K(T)$ is a direct measure of spin susceptibility, the following equation can be written:

$$K(T) = K_0 + \frac{A_{hf}}{N_A \mu_B} \chi_{spin}(T), \quad (1)$$

where K_0 is the temperature-independent chemical shift, A_{hf} is the hyperfine coupling constant, and N_A is Avogadro's number. As long as A_{hf} is constant, $K(T)$ should follow $\chi_{spin}(T)$. We estimated the exchange couplings by fitting the $K(T)$ data with Eq.(1). Here, χ_{spin} is the expression for the spin susceptibility of the $S = \frac{1}{2}$ chain model given by Johnston *et al.*⁷ which is valid in the whole temperature range of our experiment from 2 to 300 K and also in the whole limit of $0 \leq \alpha \leq 1$. The $K(T)$ data for $\text{Bi}_6\text{V}_3\text{O}_{16}$ agree well with the $S = \frac{1}{2}$ chain model with $K_0 \simeq -370$ ppm, $A_{hf} = 5.64$ KOe/ μ_B with an exchange coupling $J_1/k_B = 113(5)$ K, and the alternation ratio $\alpha = 1$ (uniform chain) and $\alpha = 0.995$ (alternating chain; Fig. 10). For the alternation ratio of $\alpha = 0.95$, the zero-field spin gap between the singlet and triplet states according to the $S = \frac{1}{2}$ alternating chain model is $\Delta/k_B \simeq 9.52$ K according to Johnston *et al.*⁷ and 10.35 K according to Barnes *et al.*,²⁰ depending on the method of approximation. Our M vs H results up to 14 T (see Fig. 6) did not show any signature of closing of the spin gap near the respective magnetic fields, which prompts us to consider that uniform chain is the correct model indeed.

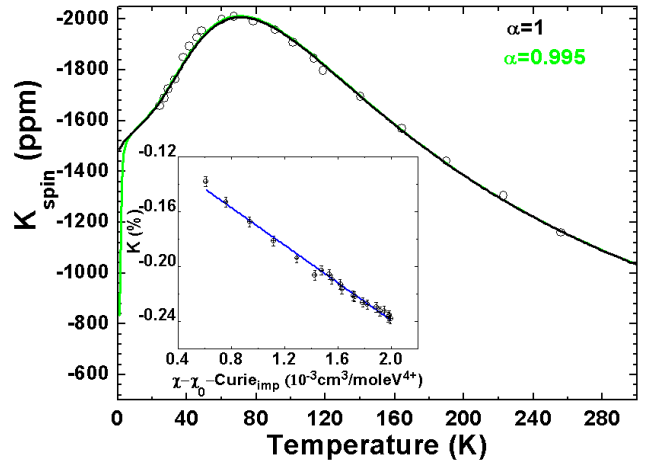


Figure 10: Temperature dependence of the ^{51}V NMR shift K of $\text{Bi}_6\text{V}_3\text{O}_{16}$ (shown by black circles) measured using the cryoMAS technique. The black and green lines are the fittings with the susceptibility model using Eq.(1) for a $S = \frac{1}{2}$ uniform chain ($\alpha = 1$) and for an alternating chain ($\alpha = 0.995$), respectively. The inset shows the ^{51}V MAS-NMR shift K of $\text{Bi}_6\text{V}_3\text{O}_{16}$ vs $\chi - \chi_0 - \chi_{Curie}$, where both $\chi(T)$ and K are measured at 4.7 T, with temperature being an implicit parameter. The solid line is the linear fit.

It is insightful to compare our results with the recently investigated uniform chain compound $(\text{NO})[\text{Cu}(\text{NO}_3)_3]$ with intrachain coupling $J = 142(3)$ K and long-range magnetic order taking place only at $T_N = 0.58(1)$ K, resulting in a ratio of suppression represented by $f = |J|/T_N = 245(10)$.¹⁶⁻¹⁸ Even more recently, a study on $\text{Cs}_4\text{CuSb}_2\text{Cl}_{12}$ reported $J = 186(2)$ K and a superconductorlike phase transition taking place only at $T_{sp} = 0.70(1)$ K, resulting in a ratio of suppression represented by $f = |J|/T_{sp} = 270(7)$.¹⁹ KCuF_3 has a relatively large interchain coupling ($J'/J \approx 0.01$), yielding $f = 390$ K/39 K = 10;¹² Sr_2CuO_3 , with a tiny interchain interaction ($J'/J \approx 10^{-5}$), gives $f = 2200$ K/5 K = 440.¹³ For $\text{Bi}_6\text{V}_3\text{O}_{16}$ the lowest estimate would be $f = 108$ K/2 K ≈ 55 , suggesting that the interchain exchange interactions here are very weak and/or frustrated.

The K vs $\chi(T)$ plot is shown in the inset of Fig. 10, where K is measured shift in percent and $\chi - \chi_0 - \chi_{Curie}$ is magnetic susceptibility without the T -independent and Curie impurity contributions. The magnetic susceptibility was measured in the same magnetic field of 4.7 T in which the NMR measurements were performed.

3. Spin lattice relaxation rate $1/T_1$

To study microscopic properties of 1D Heisenberg anti-ferromagnets (HAF), it is necessary to measure the temperature dependence of the spin lattice relaxation rate $1/T_1$, which gives information about the imaginary part

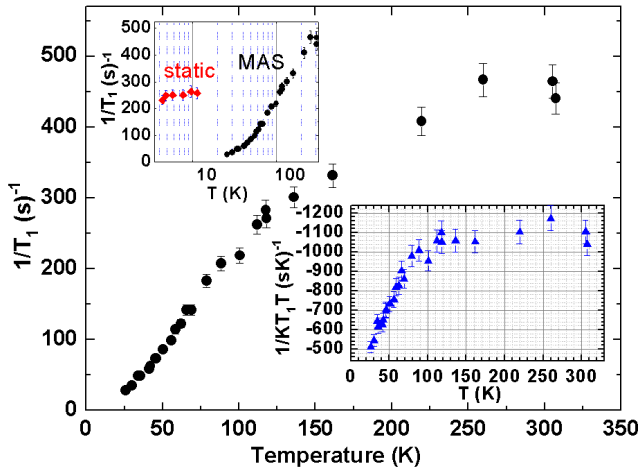


Figure 11: Temperature dependence of the spin-lattice relaxation rate ($1/T_1$) of $\text{Bi}_6\text{V}_3\text{O}_{16}$. In the top inset the same plot is shown with temperature in the log scale and low- T data measured on a static sample (red diamonds). The bottom inset shows the plot of $1/KT_1T$ vs T .

of the dynamic susceptibility $\chi(q, \omega)$. As vanadium is a $I = 7/2$ nucleus and to avoid further broadening due to dipole-dipole interaction we studied the temperature dependence of $1/T_1$ in the rotating conditions. The temperature dependence of ^{51}V $1/T_1$ is presented in Fig. 11. In the whole temperature range from 300 down to 20 K, the recovery of nuclear magnetization is single exponential. We have not observed any indication of divergence of the relaxation rate, revealing the absence of any magnetic ordering. Also, no sign of activated behavior was observed, which proves that down to 20 K no dimerization takes place. Until about 100 K, $1/T_1$ drops linearly with temperature. However, below 100 K deviations from the linear behavior are observed. Additionally, $1/KT_1T$ is temperature independent at $100 \text{ K} \leq T \leq 300 \text{ K}$, and it shows linear behavior with T below 100 K.

We did not observe any signatures of magnetic ordering, and also no features of spin gap are observed in the temperature dependence of $1/T_1$. Generally, $1/T_1$ depends on both uniform ($q = 0$) and staggered spin fluctuations ($q = \pm\pi/a$). The uniform component leads to $1/T_1 \sim T$, while the staggered component gives $1/T_1 = \text{const.}$ ⁵⁹ The deviation from the linear behavior of $1/T_1$ below 100 K presumably indicates that the temperature-independent part is coming into play which was otherwise absent in the temperature region above 100 K. This fact is also reflected in the $1/KT_1T$ vs T plot as $1/KT_1T$ is expected to be constant when the ($q = 0$) contribution dominates. In our $1/KT_1T$ plot, we observe a clear drop from the high- T constant value for temperatures ≤ 100 K.

To observe the temperature dependence of $1/T_1$ at lower temperatures, we stopped spinning and performed NMR measurements on the broad line in static conditions; $1/T_1$ below 15 K is essentially T independent. The

absolute value of the relaxation rate at low T is much larger than in cryoMAS-NMR, which seems to indicate that in the static T_1 measurements we have started to detect the magnetic V^{4+} at low temperatures with a very short relaxation (see the top inset in Fig. 11). Note that $1/T_1$ becoming constant at low temperatures is expected for $S = \frac{1}{2}$ 1D HAF systems.⁶⁰ Similar spin-lattice relaxation behavior has been observed in the uniform $S = \frac{1}{2}$ 1D chain $\text{Ba}_2\text{Cu}(\text{PO}_4)_2$.¹⁵

IV. CONCLUSION AND OUTLOOK

We have reported bulk thermodynamic and local NMR studies of the $S = \frac{1}{2}$ V-based compound $\text{Bi}_6\text{V}_3\text{O}_{16}$. All of the measurements confirm the presence of low dimensionality in this material. Upon subtracting the low-temperature Curie-Weiss contribution, the magnetic spin susceptibility agrees well with the $S = \frac{1}{2}$ uniform Heisenberg chain model. The magnetic heat capacity also confirms the existence of low-dimensional magnetism in the system, even though the lattice part has a dominant contribution to the total heat capacity, and approximation by any model is not decisive. In the MAS-NMR experiments on $\text{Bi}_6\text{V}_3\text{O}_{16}$, we observed a single sharp line which confirms that there is no site sharing between the V^{4+} and V^{5+} ions in this compound. The spin susceptibility calculated from the MAS-NMR experiments agrees well with the uniform $S = \frac{1}{2}$ chain model with the dominant exchange coupling of $J = 113(5)$ K, while the temperature variation of Knight shift agrees well with the findings from χ vs T measurements. Our experimental results from cryoMAS-NMR measurements concur with the $S = \frac{1}{2}$ uniform chain model up to the available temperature range. No sign of magnetic ordering or any feature of spin gap has been observed in the temperature dependence of $1/T_1$. $\text{Bi}_6\text{V}_3\text{O}_{16}$ is one of the very few V-based systems in the category of uniform spin chains where no long-range magnetic ordering or any singlet formation were observed above 2 K, while J is of the order of 100 K. An ideal $S = \frac{1}{2}$ spin chain cannot exist in any real material because even an infinitesimal interchain coupling would give rise to long-range magnetic order at suppressed, but finite, temperatures.

Future work involving local probe experiments, e.g. static NMR experiments down to millikelvin temperatures, neutron diffraction, muon spin resonance, etc., is needed to acquire further knowledge about the possible ordering temperature and the nature of the ordered magnetic structure of $\text{Bi}_6\text{V}_3\text{O}_{16}$, for which a high-quality single crystal is needed.

V. ACKNOWLEDGEMENT

We thank M. B. Ghag and P. N. Mundy for the help and support during the sample preparation at TIFR, A. A. Tsirlin and K. Kundu for insightful discussions,

K. Tönsuaadu for help with TG/DTA experiments and analysis, and T. Tuherm for his help during our cryoMAS measurements at NICPB. We acknowledge the Department of Science and Technology, government of

India; European Regional Development Fund (TK134); Estonian research council (PRG4, IUT23-7, MOBJD295, MOBJD449) for financial support.

-
- * Electronic address: tanmoy.chakrabarty@kbfi.ee
† Electronic address: ivo.heinmaa@kbfi.ee
‡ Electronic address: valeriy.verchenko@gmail.com
§ Electronic address: paulose@tifr.res.in
¶ Electronic address: raivo.stern@kbfi.ee
- ¹ E. Lieb, T. Schultz, and D. Mattis, *Ann. Phys.* **16**, 407 (1961).
 - ² I. Affleck, *J. Phys. Condens. Matter* **1**, 3047 (1989).
 - ³ S. Eggert, I. Affleck, and M. Takahashi, *Phys. Rev. Lett.* **73**, 332 (1994).
 - ⁴ A. Klümper and D.C. Johnston, *Phys. Rev. Lett.* **84**, 4701 (2000).
 - ⁵ J.C. Bonner and M.E. Fisher, *Phys. Rev.* **135**, A640 (1964).
 - ⁶ J.C. Bonner, H.W.J. Blöte, J.W. Bray, and I.S. Jacobs, *J. App. Phys.* **50**, 1810 (1979).
 - ⁷ D.C. Johnston, R.K. Kremer, M. Troyer, X. Wang, A. Klümper, S.L. Bud'ko, A.F. Panchula, and P.C. Canfield, *Phys. Rev. B* **61**, 9558 (2000).
 - ⁸ N.D. Mermin and H. Wagner, *Phys. Rev. Lett.* **17**, 1133 (1966).
 - ⁹ Y. Endoh, G. Shirane, R.J. Birgeneau, P.M. Richards, and S.L. Holt, *Phys. Rev. Lett.* **32**, 170 (1974).
 - ¹⁰ S.E. Nagler, D.A. Tennant, R.A. Cowley, T.G. Perring, and S.K. Satija, *Phys. Rev. B* **44**, 12361 (1991).
 - ¹¹ D.A. Tennant, T.G. Perring, R.A. Cowley, and S.E. Nagler, *Phys. Rev. Lett.* **70**, 4003 (1993).
 - ¹² B. Lake, D.A. Tennant, D. Alan, C.D. Frost, and S.E. Nagler, *Nature Materials* **4**, 329 (2005); B. Lake, D.A. Tennant, J.-S. Caux, T. Barthel, U. Schollwöck, S.E. Nagler, and C.D. Frost, *Phys. Rev. Lett.* **111**, 137205 (2013).
 - ¹³ N. Motoyama, H. Eisaki, and S. Uchida, *Phys. Rev. Lett.* **76**, 3212 (1996); K.M. Kojima, Y. Fudamoto, M. Larkin, G.M. Luke, J. Merrin, B. Nachumi, Y.J. Uemura, N. Motoyama, H. Eisaki, S. Uchida, K. Yamada, Y. Endoh, S. Hosoya, B.J. Sternlieb, and G. Shirane, *Phys. Rev. Lett.* **78**, 1787 (1997).
 - ¹⁴ M. Mourigal, M. Enderle, A. Klöpperpieper, J.-S. Caux, A. Stunault, and H.M. Rønnow, *Nature Physics* **9**, 3435 (2013).
 - ¹⁵ R. Nath, A. V. Mahajan, N. Büttgen, C. Kegler, A. Loidl, and J. Bobroff, *Phys. Rev. B* **71**, 174436 (2005).
 - ¹⁶ O. Volkova, I. Morozov, V. Shutov, E. Lapsheva, P. Sindzingre, O. Cépas, M. Yehia, V. Kataev, R. Klingeler, B. Büchner, and A. Vasiliev, *Phys. Rev. B* **82**, 054413 (2010).
 - ¹⁷ O. Janson, A.A. Tsirlin, and H. Rosner, *Phys. Rev. B* **82**, 184410 (2010).
 - ¹⁸ C. Balz, B. Lake, H. Luetkens, C. Baines, T. Guidi, M. Abdel-Hafiez, A.U.B. Wolter, B. Büchner, I.V. Morozov, E.B. Deeva, O.S. Volkova, and A.N. Vasiliev, *Phys. Rev. B* **90**, 060409(R) (2014).
 - ¹⁹ T.T. Tran, Y. Zhang, M.J. Winiarski, J. Sun, and T.M. McQueen, [arXiv: 1907.02847](https://arxiv.org/abs/1907.02847) (2019).
 - ²⁰ T. Barnes, J. Riera, and D.A. Tennant, *Phys. Rev. B* **59**, 11384 (1999).
 - ²¹ J.C. Bonner, S.A. Friedberg, H. Kobayashi, D.L. Meier, and H.W.J. Blöte, *Phys. Rev. B* **27**, 248 (1983).
 - ²² G. Xu, C. Broholm, D.H. Reich, and M.A. Adams, *Phys. Rev. Lett.* **84**, 4465 (2000).
 - ²³ D.C. Johnston, J.W. Johnson, D.P. Goshorn and A.J. Jacobson, *Phys. Rev. B* **35**, 219 (1987).
 - ²⁴ T. Barnes and J. Riera, *Phys. Rev. B* **50**, 6817 (1994).
 - ²⁵ A.W. Garrett, S.E. Nagler, D.A. Tennant, B.C. Sales, and T. Barnes, *Phys. Rev. Lett.* **79**, 745 (1997).
 - ²⁶ J. Kikuchi, K. Motoya, T. Yamauchi, and Y. Ueda, *Phys. Rev. B* **60**, 6731 (1999).
 - ²⁷ A. Zheludev, G. Shirane, Y. Sasago, M. Hase, and K. Uchinokura, *Phys. Rev. B* **53**, 11642 (1996).
 - ²⁸ N. Ahmed, P. Khuntia, K.M. Ranjith, H. Rosner, M. Baenitz, A.A. Tsirlin, and R. Nath, *Phys. Rev. B* **96**, 224423 (2017).
 - ²⁹ S. Lebernegg, O. Janson, I. Rousochatzakis, S. Nishimoto, H. Rosner, and A.A. Tsirlin, *Phys. Rev. B* **95**, 035145 (2017).
 - ³⁰ W. Zhou, *J. Solid State Chem.* **76**, 290 (1988).
 - ³¹ J. Galy, R. Enjalbert, P. Millán, and A. Castro, *C.R. Acad. Sci. Paris II* **317**, 43 (1993).
 - ³² F. Abraham, J.C. Boivin, G. Mairesse, and G. Novogrocki, *Sol. St. Ionics* **40-41**, 934 (1990).
 - ³³ V.V. Kharton, F.M.B. Marques, and A. Atkinson, *Sol. St. Ionics* **174**, 135 (2004).
 - ³⁴ B. Aurivillius, *Arkiv Kemi* **2**, 519 (1950).
 - ³⁵ C.N.R. Rao and J. Gopalakrishnan, *New Directions in Solid State Chemistry*, Cambridge University Press, New York (1987).
 - ³⁶ S. Sorokina, R. Enjalbert, P. Baules, A. Castro, and J. Galy, *J. Solid State Chem.* **125**, 54 (1996).
 - ³⁷ C. Satto, P. Millet, P. Sciau, C. Roucau, and J. Galy, *Mater. Res. Bull.* **34**, 655 (1999).
 - ³⁸ K. Momma and F. Izumi, *J. Appl. Crystallogr.* **44** 1272–1276 (2011).
 - ³⁹ O. Joubert, A. Jouanneaux, and M. Ganne, *Nucl. Instrum. Methods Phys. Res. B* **97**, 119 (1995).
 - ⁴⁰ M. Huvé, R. Vannier, G. Nowogrocki, G. Mairesse, and G. van Tendeloo, *J. Mater. Chem.* **6**, 1339 (1996).
 - ⁴¹ Y. Zhang and Y. Ueda, *Inorg. Chem.* **52**, 5206 (2013).
 - ⁴² Y. Zhang, T. Yamamoto, M. A. Green, H. Kageyama, and Y. Ueda, *Inorg. Chem.* **54**, 10925 (2015).
 - ⁴³ V. Petříček, M. Dušek, and L. Palatinus, *Z. Kristallogr.* **229**, 345 (2014).
 - ⁴⁴ D. Arçon, I. Heinmaa, and R. Stern, in *Modern Methods in Solid-state NMR: A Practitioner's Guide*, edited by: P. Hodgkinson, *New Developments in NMR Vol. 15*, (Royal Society of Chemistry, 2018) pp. 231-261.
 - ⁴⁵ A.A. Shubin, D.F. Khabibulin, and O.B. Lapina, *Catalysis Today* **142**, 220 (2009).
 - ⁴⁶ F. Delmaire, M. Rigole, E.A. Zhilinskaya, A. Aboukais, R. Hubaut, and G. Mairesse, *Phys. Chem. Chem. Phys.* **2**, 4477 (2000).

- ⁴⁷ About twice faster spinning results in higher sample temperature and smaller susceptibility and consequently slightly smaller shift value.
- ⁴⁸ F.D. Hardcastle, I. E. Wachs, H. Eckert, and D.A. Jefferson, *J. Sol. St. Chem.* **90**, 194 (1991).
- ⁴⁹ N. Kim and C.P. Grey, *Science* **297**, 1317 (2002).
- ⁵⁰ G. Mairesse, P. Roussel, R.N. Vannier, M. Anne, G. Nowogrocki, *Sol. St.Sci.* **5**, 861 (2003).
- ⁵¹ M.A. Vachon, W. Kundhikanjana, A. Straub, V.F. Mitrović, A.P. Reyes, P. Kuhns, R. Coldea, and Z. Tylczynski, *J. Phys.* **8**, 222 (2006).
- ⁵² M. Jaime, V.F. Correa, N. Harrison, C.D. Batista, N. Kawashima, Y. Kazuma, G.A. Jorge, R. Stern, I. Heinmaa, S.A. Zvyagin, Y. Sasago, and K. Uchinokura, *Phys. Rev. Lett.* **93**, 087203 (2004);
- ⁵³ S. Krämer, R. Stern, M. Horvatić, C. Berthier, T. Kimura, and I.R. Fisher, *Phys. Rev. B* **76**, 100406(R) (2007).
- ⁵⁴ S. Krämer, N. Laflorencie, R. Stern, M. Horvatić, C. Berthier, H. Nakamura, T. Kimura, and F. Mila, *Phys. Rev. B* **87**, 180405 (2013).
- ⁵⁵ H. Kageyama, K. Yoshimura, R. Stern, N.V. Mushnikov, K. Onizuka, M. Kato, K. Kosuge, C.P. Slichter, T. Goto, and Y. Ueda, *Phys. Rev. Lett.* **82**, 3168 (1999);
- ⁵⁶ K. Kodama, M. Takigawa, M. Horvatić, C. Berthier, H. Kageyama, Y. Ueda, S. Miyahara, F. Becca, F. Mila, *Science* **298**, 395 (2002).
- ⁵⁷ T. Chakrabarty, A.V. Mahajan, A.A. Gippius, A.V. Tkachev, N. Büttgen, and W. Kraetschmer, *Phys. Rev. B* **88**, 014433 (2013).
- ⁵⁸ T. Chakrabarty, A.V. Mahajan, and B. Koteswararao, *J. Phys.: Condens. Matter* **26**, 265601 (2014).
- ⁵⁹ S. Sachdev, *Phys. Rev. B* **50**, 13006 (1994).
- ⁶⁰ V. Barzykin, *Phys. Rev. B* **63**, 140412(R) (2001).